Electronic Supplementary Material (ESI) for Journal of Materials Chemistry A.

Supporting information for

Annealing-induced evolution at the $LiCoO_2$ /$LiNbO_3$ interface and its functions in all-solid-state batteries with a $Li_{10}GeP_2S_{12}$ electrolyte

Xueying Sun[a], Satoshi Hori[b], Yuxiang Li [a], Yuto Yamada [b], Kota Suzuki [a], Masaaki Hirayama [a] and Ryoji Kanno *[a, b]

[a.] *Department of Chemical Science and Engineering, School of Materials and Chemical Technology, Tokyo Institute of Technology, 4259 Nagatsuta, Midori, Yokohama 226-8502, Japan.*

[b.] *All-Solid-State Battery Unit, Institute of Innovative Research (IIR), Tokyo Institute of Technology, 4259 Nagatsuta, Midori, Yokohama 226-8502, Japan.*

***Corresponding Author:** (R.K.) E-mail: kanno@echem.titech.ac.jp

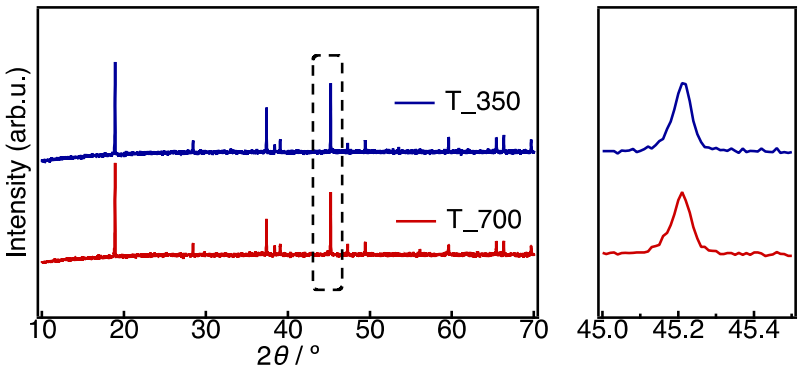

Figure S1. X-ray diffraction (XRD) patterns of LNO-coated LCOs annealed at 350 °C (T_350) and 700 °C (T_700). The XRD patterns of the LNO-coated LCO particles were acquired using an X-ray powder diffractometer (Smart lab, Rigaku) with Cu$K\alpha_1$ radiation. The data were recorded in a 2θ range of 10°–70° with a step of 0.01°. Figure S1 illustrates the XRD patterns of the LNO-coated LCO powders annealed at different temperatures. There was no significant change in the peak position for the T_350 and T_700 samples, which indicates that there was no bulk structure variation in the two samples.

Table S1. Fitting parameters for cells using LNO-coated LCO with different annealing temperatures.

Parameters	bare-LCO	T_700	T_350	T_350_700
R_0 / Ω	10	16	14	25
R_1 / Ω	63	39	21	11
C_1 / F	7.2×10^{-8}	4.9×10^{-8}	7.0×10^{-8}	4.5×10^{-8}
R_2 / Ω	4.5×10^{3}	1.7×10^{3}	18.14	23
C_2 / F	2.8×10^{-6}	1.5×10^{-6}	1.1×10^{-6}	1.2×10^{-6}
R_3 / Ω	–	–	–	61
C_3 / F	–	–	–	7.1×10^{-4}

The fitting parameters of the equivalent model for the cells are listed in Table S1. The fittings were performed using the Bio-Logic software (EC-lab). The fitting circuit is shown in Figure 4b. It contains three sets of resistance (R) and a constant phase element (CPE) in parallel. These sets of R|CPE were then connected serially with a resistance of R_0. The CPE impedance is defined by equation [S1].

$$Z_{CPE} = \frac{1}{Q(j\omega)^{\alpha}} \qquad [S1]$$

The parameter α has a value between 0 and 1. The equivalent capacitance of each set of R|CPE can be obtained by equation [S2] as follows:

$$C = R^{\left(\frac{1-\alpha}{\alpha}\right)} Q^{\left(\frac{1}{\alpha}\right)} \qquad [S2]$$

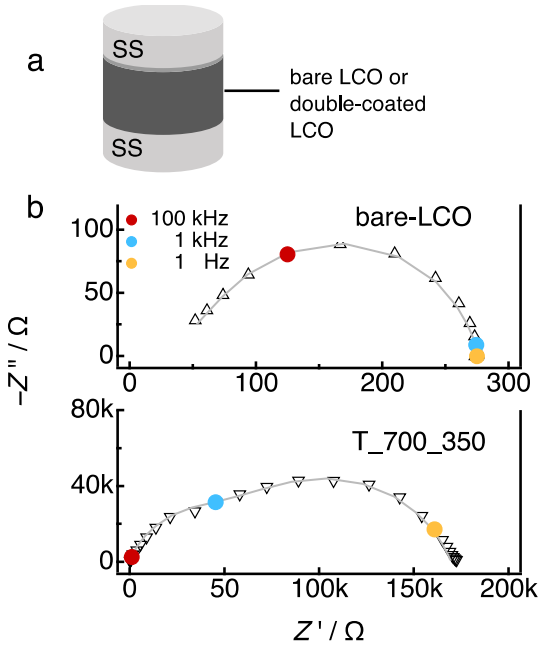

Figure S2. AC impedance measurement of bare LCO and T_700_350 pellets. (a) Pellet configuration, (b) Nyquist plots. The figure supplements Figure 5 in the main text. It demonstrates the AC impedance results for bare LCO and T_700_350 pellets. The testing methods and conditions are the same as those of the AC impedances of T_350 and T_700 in Figure 5. Combined with the data of T_350 and T_700, it was found that the bare LCO exhibited the highest electronic conductivity, whereas the double-coated T_700_350 demonstrated the lowest conductivity. These results correlate with the assertion that low-temperature-annealed LNO-coated LCO has a lower electronic conductivity than LCO, and the high annealing temperature will increase the electronic conductivity in the LNO layer.

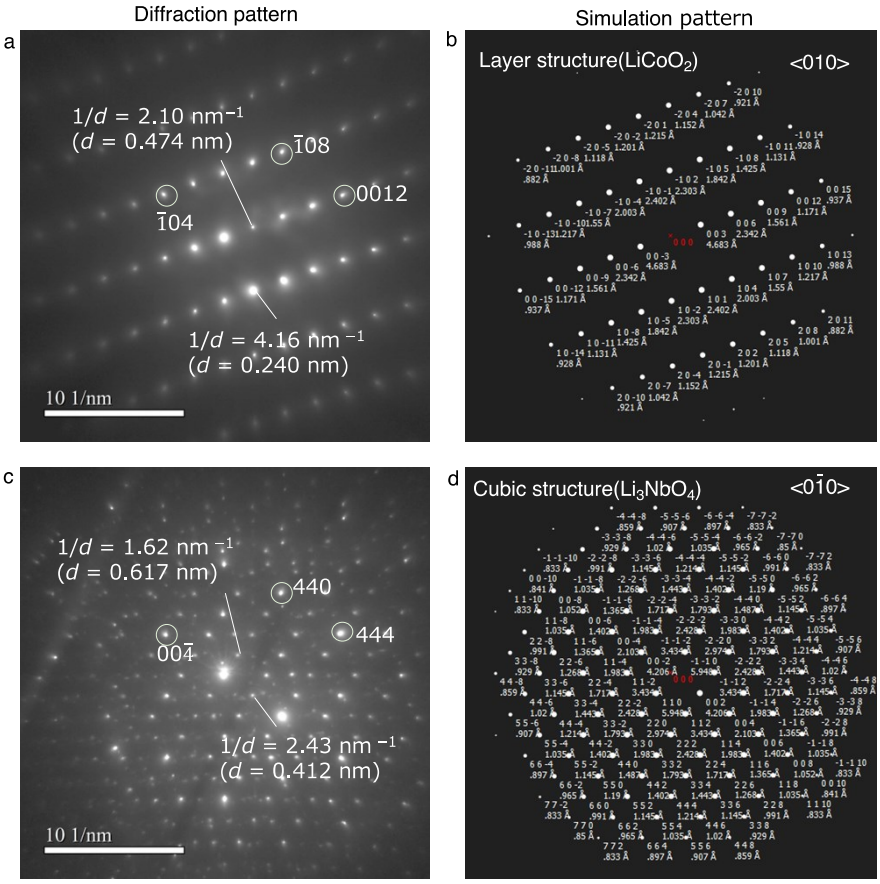

Figure S3. Diffraction patterns and the corresponding simulation patterns obtained by STEM analysis for the T_700 sample. (a) Diffraction pattern of a region in the bulk area, which is approximately 1 μm away from the particle boundary, and (b) the corresponding simulation pattern for (a), indicating a layered $LiCoO_2$-type structure. (c) Diffraction pattern of a spot on the particle boundary, and (d) the corresponding simulation pattern for (c), indicating a cubic Li_3NbO_4-type structure. Information on the diffraction and simulation patterns of the crystal structure for the T_700 sample are shown in Figure S3. This figure supplements Figure 7, revealing a detailed structural change. Panels (a) and (b) display the diffraction pattern of the LCO side and its corresponding indexed simulation pattern, respectively, indicating that the structure of the material on the LCO side remains a $LiCoO_2$-type structure. In contrast, at the LNO side, the diffraction pattern in (c) clearly indicates a crystallised structure that can be determined by the simulation pattern in (d). The results suggest that the amorphous LNO layer transformed into Li_3NbO_4-type crystals after

annealing at 700 °C.

Table S2. XPS analysis-derived Co and Nb elements atomic concentrations.

Samples	Co content /at%	Nb content /at%	Co:Nb ratio
T_350	0.4	2.0	1:5
T_700	3.2	3.1	1:1

Table S2 lists the detailed values with regard to the XPS spectra shown in Figure 9a in the main text. For the data analysis of the XPS spectra displayed in Figure 9a, the peak locations and widths were obtained using Shirley background subtraction and by fitting the data with mixed Gaussian-Lorentzian line shapes using the CasaXPS software package. Table S2 demonstrates that the Co concentration in the surface layer of T_700 is four times higher than that on the surface of T_350, indicating the surface atomic rearrangement and Co diffusion to the surface during the annealing process at 700 °C.

Table S3. Fitting parameters used for the XPS analysis shown in Figure 10.

		O			Nb				S				
	Component	A	B	C	D		Component	E		F	G	
bare-LCO	Binding energy /eV	529.6	532.0	–		LGPS	Binding energy /eV	161.1	162.3	163.5		
	FWHM / eV	1.0	2.1	–			FWHM / eV	1.7	1.6	1.3		
	Relative composition	46.4	45.5	–			Relative composition	65.2	32.6	2.2		
T_350	Binding energy / eV	529.6	531.6	533.2	206.6	209.3	T_350 +LGPS	Binding energy / eV	161.1	162.4	163.7	166.7	169.0
	FWHM / eV	1.8	1.7	1.6	1.6	1.4		FWHM / eV	1.3	1.3	1.4	0.8	2.8
	Relative composition	38.5	38.0	23.6	60.0	40.0		Relative composition	58.4	29.2	4.0	1.1	7.3
T_700	Binding energy / eV	529.7	531.9	–	207.7	209.5	T_700 + LGPS	Binding energy / eV	160.9	162.1	162.9	166.6	168.7
	FWHM / eV	1.1	2.2	–	1.2	1.2		FWHM / eV	1.2	1.2	2.1	0.9	2.1
	Relative	50.39	43.1	–	60.0	40.0		Relative	46.4	23.2	15.8	22.3	12.4